Bone 69 (2014) 109–117

Contents lists available at ScienceDirect

Bone

journal homepage: www.elsevier.com/locate/bone

Original Full Length Article

Rapid alterations of avian medullary bone material during the daily egg-laying cycle

Michael Kerschnitzki [a,1], Thomas Zander [a,2], Paul Zaslansky [b], Peter Fratzl [a], Ron Shahar [c], Wolfgang Wagermaier [a,*]

[a] Max Planck Institute of Colloids and Interfaces, Department of Biomaterials, Potsdam, Germany
[b] Charité Universitätsmedizin Berlin, Julius-Wolff-Institute, Berlin, Germany
[c] The Hebrew University of Jerusalem, Laboratory of Bone Biomechanics, Rehovot, Israel

ARTICLE INFO

Article history:
Received 7 May 2014
Revised 27 August 2014
Accepted 28 August 2014
Available online 6 September 2014

Edited by: David Burr

Keywords:
Medullary bone
Oviposition cycle
Bone remodeling
Calcification
Mineral particle properties
X-ray diffraction

ABSTRACT

Bone is a dynamic tissue which is continuously adapting not only to external mechanical stimuli but also to internal metabolic calcium demands. During normal bone remodeling, bone-resorbing osteoclasts release calcium from the bone and digest the collagenous bone matrix, after which bone-depositing osteoblasts form unmineralized collagen matrix, which subsequently mineralizes. The detailed mechanism by which calcium is deposited at the site of mineralization and removed from it during bone resorption is largely unknown. Experimental studies are difficult to conduct because in adult bone only a small fraction of bone tissue is remodeled at any moment in time. Thus, one promising approach is to study mineral deposition and resorption in model systems in which a large fraction of the bone mineral is mobilized in a relatively short period of time. We investigated the microscopic and nanoscopic alterations of avian medullary bone architecture during the egg-laying (oviposition) cycle of hens. Medullary bone forms a labile calcium reservoir for eggshell production and is characterized by an extremely rapid and high-flux calcium metabolism. It thus, provides the unique opportunity to study processes of bone remodeling in their most intensive form. We used a combination of synchrotron X-ray tomography together with small angle X-ray scattering (SAXS), wide angle X-ray diffraction (WAXD) and X-ray fluorescence (XRF) to correlate microscopic medullary bone attributes such as the mineral content, medullary bone volume fraction and medullary bone trabecular thickness with nanoscopic alterations in the mineral particle size (thickness parameter T and length parameter L) during the oviposition cycle. To identify the timing of the different stages of the cycle, ionic calcium, phosphorus and PTH concentrations in the blood of the layers were monitored.

We found that the microscopic and nanoscopic architecture of avian medullary bone material changes rapidly during the oviposition cycle. During eggshell calcification, the mineral content and the size of trabeculae of medullary bone decrease markedly. Furthermore, the average mineral particle size increases during resorption, suggesting that the smaller mineral particles are preferentially removed. Medullary bone thus formes a fast-responding system exhibiting rapid alterations of the material at the micron and nano scale. Those mechanisms are crucial to provide calcium for the high metabolic calcium demand during eggshell mineralization.

Introduction

Bone material appears to be designed to function under varying environmental conditions that go far beyond the need to serve protection and load bearing purposes. It also fulfills metabolic functions such as maintaining body's calcium reservoir [1]. During growth and maturation, bone constantly undergoes (re)modeling. The rates of bone formation and resorption together with the kinetics of bone mineralization determine the distribution of mineral in the bone tissue [2] and thus, are characteristic for bone tissue in both health and disease [3].

During the process of bone formation, osteoblasts deposit an organic matrix – consisting of collagen and a series of non-collagenous proteins and lipids – which subsequently mineralizes. The mineral which is in a disordered calcium phosphate phase is translocated to the mineralization front where it is later transformed into more ordered phases [4–7]. After nucleation, hydroxyapatite crystals grow longitudinally to form platelets with an average length and width of 50 × 25 nm [8,9] and subsequently

* Corresponding author at: Max Planck Institute of Colloids and Interfaces, Potsdam-Golm Science Park, Am Mühlenberg 1, 14476 Potsdam, Germany.
E-mail address: wagermaier@mpikg.mpg.de (W. Wagermaier).
[1] Present Address: Weizmann Institute of Science, Department of Structural Biology, Rehovot, Israel.
[2] Present Address: Helmholtz-Zentrum Geesthacht, Institute of Materials Research, Geesthacht, Germany.

http://dx.doi.org/10.1016/j.bone.2014.08.019

in thickness of 1.5 nm to 4.5 nm — depending on species, age and tissue type [10,17]. During bone resorption, osteoclasts form a sealed highly acidic zone at the bone surface, dissolving bone mineral and decomposing the collagenous bone matrix. Bone resorption products are removed from the resorption site via transcytosis [11,12] to the basolateral region of the osteoclast where they are eventually released [13].

The most favorable circumstances to study the processes of bone formation and resorption during bone remodeling are when they occur under extreme conditions. Such a situation can be found during the daily egg-laying (oviposition) cycle in hens, in which calcium metabolism is extraordinarily intense. Commercial layers transfer about 10% of their total body calcium volume daily to the shell producing machinery in their oviducts, of this only about 50% originates from dietary sources. They are therefore the most efficient calcium transporters among all vertebrates [14]. Such an intensive transport mechanism imposes severe demands on ionic calcium homeostasis. During production of the eggshell which mainly consists of calcium carbonate, considerable amounts of the required calcium (20–40%) must be derived from skeletal reserves [15]. To accommodate this, the function of the osteoblasts changes from laying down cortical bone to producing a spongy bone termed medullary bone [22]. This bone type, unique to birds and dinosaurs [18], has no major mechanical function [19] but serves as a labile calcium source for eggshell formation. Medullary bone is laid down within the medullary cavity of the mid-diaphysis of the long bones, particularly those of the legs [19,22]. Thus, medullary bone is distinct from cancellous bone which is concentrated towards the metaphysis/epiphysis having important mechanical functions for the integrity of the whole bone structure [20,21].

During the 24 h oviposition cycle, medullary bone builds up rapidly throughout the inactive stage of egg shell mineralization at night [23,22] and during the early stages in the morning after oviposition when hens consume calcium-rich food. At the onset of mineralization of the new eggshell calcium from medullary bone reserves is released and transported to the oviducts, where it forms the calcium carbonate eggshell [15]. To date there are no studies describing the alteration of microscopic and nanoscopic mineral properties of medullary bone material in relation to the oviposition cycle. Thus, it is unclear how such high rates of calcium storage and mobilization can be facilitated and if medullary bone material shows certain adaptations in its architecture to meet these requirements.

In this work we attempt to answer these questions by investigating the dynamics of microscopic and nanoscopic structural changes in avian medullary bone material during the oviposition cycle, observed in commercial layers. We monitored serum concentrations of ionic calcium and phosphorus as well as parathyroid hormone (PTH) during the different stages of the oviposition cycle. We studied the 3D architecture and mineral content of representative samples of medullary bone by synchrotron X-ray tomography. Furthermore we used synchrotron small angle X-ray scattering (SAXS), wide angle X-ray diffraction (WAXD) and X-ray fluorescence (XRF) to characterize the ultrastructure of medullary bone material together with alterations in the mineral particle size (thickness parameter T and length parameter L) during the oviposition cycle.

Materials and methods

Samples

Egg laying hens were euthanized at the Hebrew University of Jerusalem, Israel. Ethics approval for all procedures to be carried out was obtained from the Committee for Ethics in Research of the Hebrew University of Jerusalem. At predetermined time points as detailed below, hens were euthanized by intravenous injection of an anesthetic overdose (80 mg/Kg, pentobarbital sodium (200 m/ml), CTS, Israel). Both femur bones were collected at 13 different points in time according to the oviposition cycle, starting from 0 h (directly after oviposition), and every 2 h thereafter up to 24 h after oviposition ($n = 2$ per time point). We thus obtained bones from a total of $n = 26$ animals with precisely timed bone states following oviposition. Blood samples were obtained from each hen before euthanasia, to determine serum calcium, phosphorus ion and PTH concentrations during the oviposition cycle. To improve statistics for blood analysis, blood samples from additional animals were obtained, but no bone samples were tested. Statistical significance was tested using ANOVA with subsequent post hoc tests. A statistical significant difference ($P < 0.05$) is denoted with an asterisk.

After harvesting, bone samples were stored dry in a freezer at −20 °C until further anhydrous processing, except for samples taken immediately for fresh IR analysis. Transverse slices ~1 cm thick were cut with a low speed diamond saw (IsoMet, Buehler GmbH, Düsseldorf, Germany) from the mid-diaphysis of each bone and were embedded in PMMA. Samples were dehydrated in 100% ethanol (3 times per day) for a total of 2 days and subsequently immersed in methyl methacrylate (MMA). Finally, the samples were embedded in covered plastic containers with PMMA solution containing 400 ml MMA, 100 ml nonylphenyl-polyethyleneglycol acetate (NPA) and 10 g dibenzoyl peroxide (BPO). During embedding the samples were placed in an oven at 42 °C for 12 h, 48 °C for an additional 12 h and finally at 58 °C for 24 h for hardening.

Electron microscopy

Thin transverse cross sections with a thickness of approximately 200 μm were cut from the embedded bone blocks and polished to a final thickness of approximately 50 μm. Samples were glued on an object holder with double-sided tape and mounted on aluminum stubs. A FEI-Quanta 600FEG electron microscope (FEI Company, Oregon, USA) was used in low vacuum mode (0.75 Torr) at a working distance of 10 mm. Images were taken with a solid state detector (SSD) at 15 kV acceleration voltage measuring the back-scattered-electron signal.

IR-spectroscopy

The freshly dissected pieces of medullary bone were washed with acetone to remove fatty tissue components. Samples were subsequently crushed in an agate mortar with sodium hypochlorite solution (6%) added for 5 min at room temperature. The suspension was then transferred into Eppendorf tubes and centrifuged at 14,000 rpm for 3 min in a micro centrifuge (Eppendorf 5417C, Hamburg, Germany) to remove the supernatant. The pellet was washed three times with double distilled water saturated with calcium and phosphate and twice with 100% ethanol. The pellet was resuspended in ethanol and sonicated (Ultrasonicprocessor W-380; Heat Systems Ultrasonics, Newtown, USA). The re-suspended medullary bone mineral particles were subsequently exposed to a heat lamp in order to remove the remaining ethanol. The residual bone mineral was lightly crushed in an agate mortar, mixed with potassium bromide (KBr) and a 7-mm pellet was prepared. The IR-spectra were measured with a Nicolet 380 FTIR spectrometer (Thermo Scientific, USA). The splitting factor of the phosphate υ_4 peak describing the crystallinity of the bone material was calculated following Weiner and Bar-Yosef [24].

Synchrotron X-ray scattering measurements

Thin transverse bone cross-sections with a thickness of approximately 50 μm were measured at the μSpot beamline at BESSY II (Helmholtz Zentrum Berlin für Materialien und Energie, Berlin, Germany) with a monochromatic X-ray beam of 15 keV and a beam size of $30 \times 30\ \mu m^2$. In order to obtain high q-resolution a silicon-111 double monochromator was used. A sample to detector distance of ~300 mm was used for diffraction measurements with a 2D position-sensitive CCD-detector (MarMosaic 225, Evanston, USA) with 3072×3072 pixels and a

corresponding pixel size of 73.2 μm × 73.2 μm. Bone samples were translated with an xyz precision stage allowing us to map large and well-defined areas of the bone with a spatial resolution of 30 μm. Additionally an X-ray fluorescence (XRF) detector (ASAS-SDD, KETEK Germany) was used to measure the calcium fluorescence signal simultaneously. For data correction due to X-ray absorption of the sample, the transmission intensity of each scan point was measured with a diode before each scan. The exposure time for the transmission measurements was set to 0.3 s and exposure times for diffraction (small angle X-ray scattering = SAXS and wide angle X-ray diffraction = WAXD) were set according to the sample thickness and the X-ray beam intensity and ranged between 4 and 30 s per scanning point. A detailed description of the beamline can be found elsewhere [25]. The determination of mineral particle thickness (T parameter) is based on SAXS patterns and is described in detail in [26], while mineral particle length (L parameter) is based on WAXD measurements and described e.g. in [27]. Statistical significance was tested using ANOVA with subsequent post hoc tests. A statistical significant difference ($P < 0.05$) is denoted with an asterisk. Information about shape and arrangement of the mineral platelets is contained in a rescaled function G(x) of the dimensionless parameter $x = qT$. A detailed description of G(x) can be found in [16]. Variations in species, bone age or the volume fraction of mineral lead to different shape and arrangement of the mineral particles within the collagen fibrils and furthermore to systematic differences in G(x) being clearly visible in the shape of the curve [6].

High resolution (~1 μm) XRF measurements were collected separately at the microfocus beamline ID 13 at the European Synchrotron Radiation Facility (ESRF) in Grenoble, France. A monochromatic X-ray beam with an energy of 14 keV and a beam size of 1 μm was used. Medullary bone samples were attached to a scanning stage that was translated perpendicularly to the beam, with a step size of 1 μm. The X-ray fluorescence signal was obtained with an XRF detector which was situated approximately 20 mm behind the sample at an angle of 90° to the X-ray path.

Quantitative computer micro-tomography

Medullary bone samples from 7 chickens at 4 different time points (0, 6, 18 h after oviposition 2 samples each; 12 h 1 sample) were scanned by quantitative computed tomography using a 23 keV X-ray beam at the BAMline at BESSY II Helmholtz-Zentrum Berlin für Materialien und Energie, Berlin, Germany. PMMA-embedded blocks with an approximate side length of 1 cm were mounted on the beamline sample rotation stage. To ensure absorption imaging with minimal phase-contrast enhancement at edges, the sample to detector distance was set to a minimal possible distance of 15 mm. For each sample a total of 1200 projections were measured with an effective pixel resolution of 4.348 μm. A more detailed description of the beamline setup can be found elsewhere [28]. For post-processing, the projection images were normalized using inhouse custom-written octave code and were reconstructed using the ESRF public-domain code of PyHST [29]. The reconstructed datasets were evaluated to estimate the trabecular thickness, mineral density and medullary bone volume fraction (ratio of medullary bone volume to total volume = BV/TV) using the BoneJ plugin [30] for ImageJ (National Institutes of Health, USA). For this the bone marrow space featuring the medullary bone was segmented manually to discriminate the cortical bone material from medullary bone structures.

Results

Analysis of blood samples

The analysis of blood samples of hens obtained during the oviposition cycle (Fig. 1) provides information about their daily calcium and phosphorus metabolism. This is particularly important in order to understand the temporal pattern of the ultrastructural changes of medullary bone material which served as the main calcium reservoir for eggshell production. In the early stage of the oviposition cycle (in our animals this occurred between 5 am to 11 am), the hens absorbed large amounts of calcium from their food. 6 h following oviposition, calcification of the new eggshell starts, as seen by examination of eggs present in the oviducts in hens sacrificed at that time (data not shown). During early stages (until 9 h after oviposition), ionic calcium concentration in the serum increases, and peaks before the calcification of the new egg starts (Fig. 1a). Throughout that period, serum phosphorus concentration is relatively low (Fig. 1b). During later stages (9–21 h after oviposition) ionic calcium concentration significantly decreases as the calcium resorbed from medullary bone structures is subsequently transported to the oviducts to form the eggshell which consists of calcium carbonate. However, phosphorus which is not needed for the production of the calcium carbonate eggshell remains in the blood which leads to an increase of the phosphorus concentration that peaks after around 12 h. The parathyroid hormone (PTH) concentrations (Fig. 1c) reveals that PTH expression – which is known to promote bone remodeling – appears to be significantly lower during the night (latest stage: 15 to 21 h) indicating a resting phase (inactive phase) with substantially less medullary bone resorption.

Distinct bone types in chicken long bones and mineral organization

Examination of the ultrastructure of chicken long bones shows three different bone types with clearly distinguishable spatial mineral particle arrangements. Back-scattered electron imaging on cross sections of the femoral midshaft shows the spongy medullary bone encased by compact cortical bone, which forms the outer shell of the femur (Fig. 2a, b). High magnification scans, interestingly, show some areas inside the bone marrow adjacent to medullary bone trabeculae featuring high electron densities which is associated with increased calcium content (Fig. 2c, d). These areas we term 'calcium halos' (CH) in the following analyses. Using SAXS and calcium XRF confirms that calcium is abundant in the marrow space, in areas where there is no regular 'bone structure' present (Fig. 3b). In those areas, no diffraction patterns were obtained, which excludes the presence of crystalline mineral. The characterization with SAXS reveals a different mineral particle organization in the different bone types (Fig. 3c). Mineral particles in medullary bone material are less organized as compared to those found in cortical bone, as indicated by the broader peak at lower x values in the G(x) plot. The calcium halo areas show no peak in the G(x) plot, indicating rather heterogeneous, disordered mineral particles. Infrared spectroscopy measurements show significantly lower mineral crystallinity of ~2.55 in medullary bone material as compared to the cortical bone mineral crystallinity which was measured to be ~2.75 (Fig. 3d). To better understand the calcium halos present in the bone marrow space, we used high resolution SAXS (Fig. S1 a) and XRF mapping (Fig. S1 b–c). The data show that the calcium concentration gradually decreases from the surface of the medullary bone structures to the bone marrow. However, calcium-rich aggregates are also visible inside the bone marrow space (Fig. S1b). Moreover, iron (Fig. S1 c), copper and zinc (Fig. S1 d) are also highly abundant in the bone marrow space; these are known to be important for various metabolic needs of the laying hen, such as medullary bone development or the synthesis of plasma proteins [31].

Alteration of microscopic medullary bone attributes during the oviposition cycle

To gain insight into the dynamics of medullary bone material on the micron scale, quantitative computer tomography was performed on bone sections from two animals per time point (except 12 h), using a monochromatic synchrotron beam (Fig. 4). Qualitative comparison of representative images of medullary bone material at different time

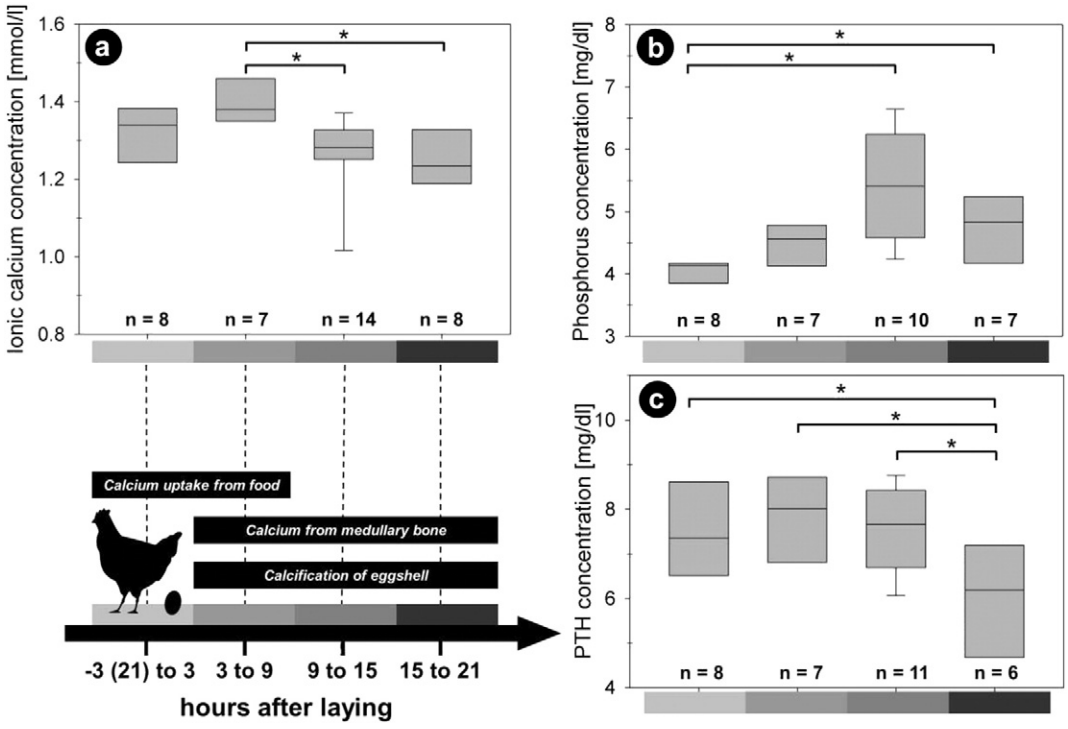

Fig. 1. Analysis of blood samples of hens obtained during the oviposition cycle: (a) Ionic calcium concentration in blood is increased in the early stages (till 9 h) after laying due to uptake of calcium rich food in that period. During later stages (9–21 h after laying), the amount of ionic calcium in the blood significantly decreases, as the eggshell calcifies. (b) Phosphorus concentration in blood increases significantly during the later stages, indicating that medullary bone material is resorbed for eggshell production. Calcium is subsequently transported to the oviducts to form the eggshell which consists of calcium carbonate. However, residual phosphorus (not used for eggshell production) remains in the blood. (c) Parathyroid hormone (PTH) concentration, which is a marker for bone remodeling is significantly decreased during the latest stage (resting phase) of the oviposition cycle. * denotes a statistically significant difference ($P < 0.05$).

points of the oviposition cycle show differences in the medullary bone architecture, namely the medullary bone volume fraction and the thickness of trabeculae (Fig. 4a). On average, bone trabeculae appear to be thicker during the early stages of the oviposition cycle (0, 6 h) and their thickness decreases during the later stages (12, 18 h) (Fig. 4c). Accordingly, BV/TV appears to be continuously decreasing during the egg-laying cycle. Both observations are the result of resorption of the trabecular structures during calcium withdrawal (Fig. 4d).

Due to the monochromatic attributes of the synchrotron imaging beam setup, the attenuation signal is not affected by beam hardening such that the spatial distribution of the attenuation coefficients and hence mineral density of the medullary bone material can be quantitatively determined. By measuring the mineral content of the medullary bone material at different time points following oviposition, we thus reveal the dynamics of medullary bone mineralization during the oviposition cycle. Fig. 4b shows distributions of the attenuation coefficient of medullary bone material (1 animal per time point) and it can be seen that throughout the whole cycle, large amounts of low mineralized tissue (material at lower values of the attenuation coefficient) are present. This certainly is linked to the calcium halos (Fig. 3) that we observed by other methods and thus hints to the existence of a high bone turnover with highly abundant immature (less mineralized) bone material. However, during the early stages, the mineral content of medullary bone trabeculae is relatively high and increases from 0 h to 6 h after oviposition. At later stages (12, 18 h) during calcium withdrawal from medullary bone, its mineral content is substantially decreased.

Temporal changes to the mineral particle size during the oviposition cycle

From the SAXS measurements at every sampled timepoint, we determined the medullary bone mineral particle size which we associate with calcium withdrawal during eggshell production (Figs. 5, 6). For each time point bone sections from two animals (except 6 h) were scanned and the histograms (Fig. 5) as well as the average in each animal per time point (Fig. 6) of the mineral particle thickness (T) and length parameter (L) were calculated. Throughout the whole cycle the mineral particle thickness parameter was found to remain relatively constant (Figs. 5a, 6a), whereas the particle length changes substantially (Figs. 5c, 6b). The histograms were grouped into two fractions of 'thick' versus 'thin' and 'long' versus 'short' mineral particles by setting thresholds of 2.2 nm and 22 nm for the thickness and length, respectively. These thresholds were chosen based on the bimodal distribution observed after plotting the histograms of all T and L values from all time points (see Supplementary Fig. S2). The relative change observed in these two fractions of the T and the L parameter is depicted in Figs. 5b and d. These results suggest that the mineral particle thickness is relatively constant during the entire oviposition cycle, whereas the mineral particle length varies significantly, peaking at about 12 h after oviposition. Fig. 6c, d shows the dynamics of the mineral particle aspect ratio (T/L) comparing the L vs. the T parameter ratios for each time point (Fig. 6c) versus the average aspect ratio (L/T) per time point and animal (Fig. 6d). The mineral aspect ratio is highest ($L/T = 10–15$) at about 12 h after oviposition, as compared to the other time points with values between 9 and 11 (Fig. 6d).

Discussion

In this study we reveal the dynamics of the oviposition cycle of hens on several length scales. In particular we (i) monitored serum levels of ionic calcium, phosphorus and PTH (macro scale) which we correlate with the amount of medullary bone (volume fraction) together with the mineral content of medullary bone structures (micro scale) due to the corresponding stage of oviposition. (ii) Furthermore we find mineral in the marrow space (calcium halos) which is present during all stages of the oviposition cycle (micro scale). (iii) Finally we measured the

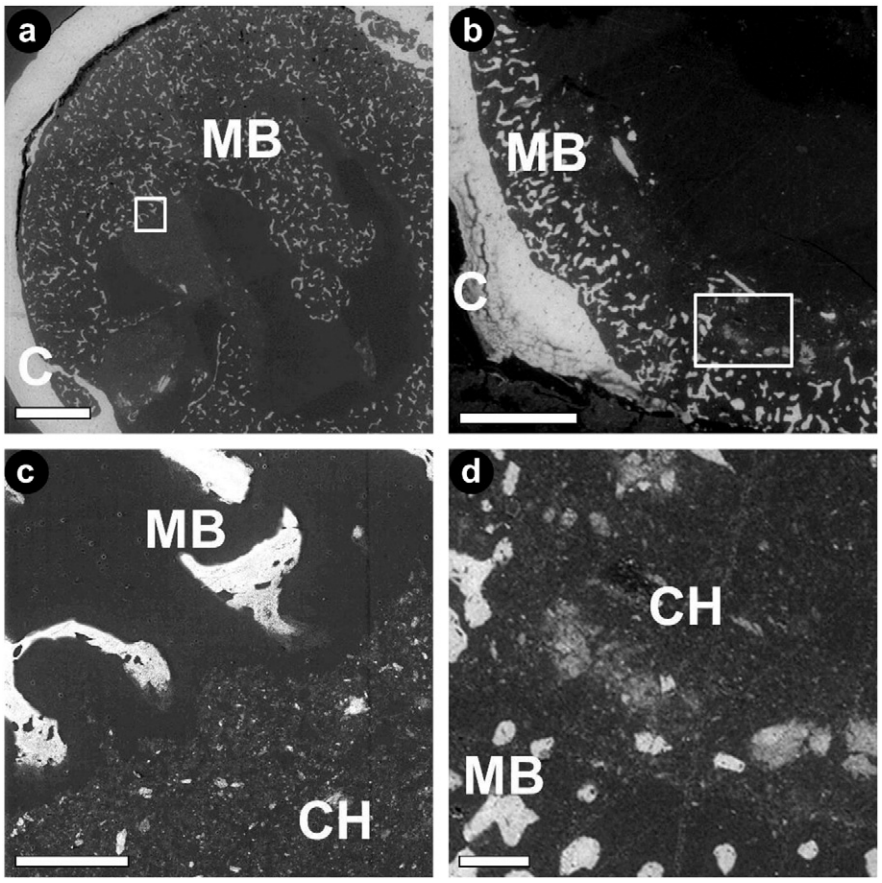

Fig. 2. Back-scattered electron micrographs exhibit the bone types present in the chicken long bone. (a & b) Low magnification images showing the compact cortex (C) and the spongy medullary bone type (MB), filling the medullary cavity. (c & d) High magnification images (box in a & b) revealing broad electron dense regions in the marrow space between medullary bone trabeculae which we refer to as 'calcium halos' (CH). Scale bars are (a & b) 1 mm, (c & d) 100 μm.

alteration of medullary bone mineral particle size (thickness and length) together with particle arrangement (nanoscale) during the oviposition cycle.

(i) During the early stages of the laying cycle, hens consume calcium-rich food which leads to a net increase of ionic calcium in the blood which reaches a peak about 6 h after oviposition. Analysis of the alteration of medullary bone morphology and mineral density with quantitative computed tomography shows that during this stage the degree of mineralization of medullary bone structures markedly increases. However, the trabecular thickness and BV/TV ratios do not change significantly. After the onset of calcification of the new eggshell (at 6 h after oviposition) ionic calcium decreases while an increase of phosphorus is seen, which is in agreement with the findings of a previous study in which calcium levels of layers were determined with a calcium-sensitive electrode [32]. Furthermore we found that medullary bone structures show distinctly decreased mineral content together with substantial changes in trabecular thickness and BV/TV ratios. It is known, that during this stage the number of active osteoclasts attached to the bone increases [34,33]. These data suggest that after the onset of calcification of the new eggshell (active stage) calcium used for eggshell production is mainly mobilized by resorption of medullary bone material [32]. We speculate, that the residual phosphorus which is not used for eggshell production must remain in the blood or it may be essential for the transport of large amounts of calcium in the form of polyphosphates [35].
Analysis of layers' blood shows that during all stages of the oviposition cycle (but not during the inactive stage which occurs during the night) PTH levels are elevated, as also shown by others [36]. It is known that PTH stimulates calcium mobilization from the medullary bone and thus promotes bone resorption [37,38]. This is supported by our tomographic data, which show that medullary bone trabecular thickness and mineral content decrease when PTH is elevated. During the resting phase when PTH levels are lower, trabecular thickness and mineral content increase again.
We want to point out that the conclusions based on our tomography data in particular on the medullary bone trabecular thickness and the BV/TV ratios are limited by the sample size of $n = 5$ femurs of different animals. The variability between duplicates is high and the statistical significance can't be tested due to the small sample size. Future experiments are necessary to verify, that the observed alteration of the bone architecture on the micron scale is indeed a result of calcium withdrawal from medullary bone structures during the oviposition cycle and not only due to the biological variability in our tested samples.

(ii) Interestingly we observe at each time point during the oviposition cycle the presence of large amounts of tissue with relatively low degree of mineralization, which indicates high bone turnover. This tissue may represent very young, freshly deposited bone material which needs to be further mineralized during the inactive period [23]. However, we also find relatively large amounts of calcium present in the bone marrow space, adjacent to medullary bone material not showing any crystalline diffraction signature. These calcium halos show a disordered mineral particle arrangement at the nanometer scale, which could be attributed to variations in lateral spacing and degree of order in the stacking of the particles [16]. Yet we can neither draw firm conclusions on the structure nor the phase of this mineral. We also do not know

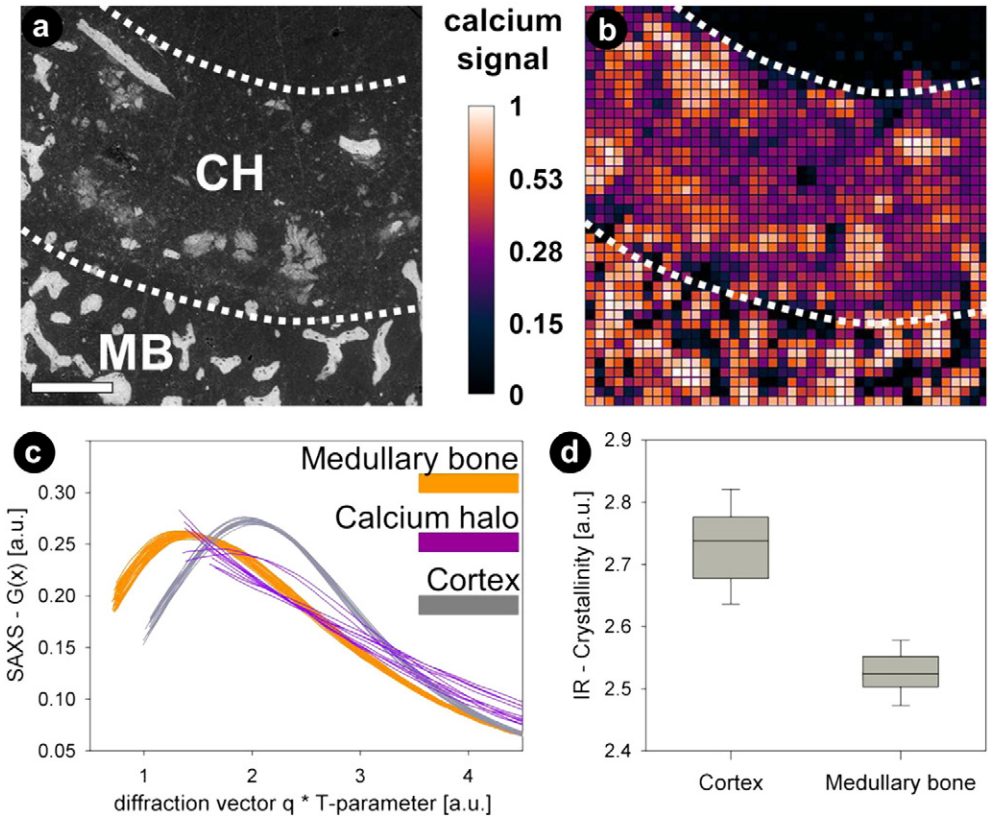

Fig. 3. Characterization of different bone types with small angle X-ray scattering and X-ray fluorescence: (a) back-scattered electron micrograph showing medullary bone trabeculae (MB) and the calcium halo (CH). Scale bar is 250 μm. (b) X-ray fluorescence mapping of the calcium concentration in the same area with a spatial resolution of 30 μm. Calcium is present in the marrow space between medullary bone trabeculae (electron dense areas denoted with the white dotted lines). (c) G(x) curves derived from the SAXS-patterns characterizing the degree of order and orientation between the mineral particles. Mineral in cortical bone is relatively homogeneous and highly organized (clear peak at higher x values). Medullary bone shows a lower degree of mineral organization denoted by the broader peak at lower x values. The 'calcium halo' shows no peak in the G(x) plot indicating a disordered mineral particle organization. (d) Crystallinity of bone mineral measured with IR-spectroscopy. Medullary bone material shows significantly lower mineral crystallinity of ~2.55 as compared to cortical bone material ~2.75 implying the presence of a less ordered mineral phase.

if this mineral is present due to prior bone resorption by osteoclasts [12,13,39] and will be further transported to the oviducts for eggshell mineralization. Alternatively it could be also used for re-mineralization of medullary bone structures during the inactive period [23,22]. However, further investigation of these calcium halos might help to better understand the pathways of bone formation and resorption in particular the mineral phases as well as the transport and stabilization mechanisms involved in these processes as those are to date still ambiguous [40,41].

(iii) At the nanoscopic level we only observe little alteration in the average thickness of medullary bone mineral particles mostly pronounced during the latest stage of the oviposition cycle. However the mineral particle length shows a distinct trend with the longest particles found during the later stages of the laying cycle. Furthermore we observe two distinct species of mineral particles in terms of their length. The fraction of long particles continually increases during the oviposition cycle with the biggest fraction of long mineral particles (thus highest aspect ratio) found just before the resting phase at night. This finding shows that during mobilization of medullary bone mineral, short mineral particles are resorbed faster and predominantly longer mineral particles remain in the bone tissue leading to an increase of the measured average bone mineral length. During the resting phase, the average mineral particle length decreases indicating the formation of new mineral crystals which subsequently grow in length but show a rather constant particle thickness. This may indicate that after deposition of young bone matrix, the hydroxyapatite mineral crystals quickly grow along the longitudinal direction but only slowly in thickness. Similar mineral particle growth dynamics were also observed in postnatal murine long bone development during which mineral particles predominantly grow in length [27].

Our data also shows that medullary bone mineral significantly differs from the cortical bone of the laying hens. We found that the cortical bone shows a higher mineral concentration than medullary bone, supporting the findings of others [19]. Moreover our findings show that cortical bone mineral is more highly organized, shows higher mineral crystallinity and features significantly thicker and longer mineral particles. Note that the relation between the mineral particle size (measured with X-ray techniques) and the IR — crystallinity determined by the splitting of the phosphate υ_4 peak: The υ_4-splitting describes the different vibration behavior of phosphate groups inside the bone mineral. It thus describes the extent to which the atoms in the mineral lattice are ordered as well as the ratio between phosphate groups at the surface and in the bulk of the mineral particles – in other words – the relative size of the mineral crystals [24]. The different structural characteristics of medullary bone compared to the cortical bone may be one of the reasons why medullary bone can be metabolized at a rate 10–15 times faster than the cortical bone [42,43]. On the microscopic scale it indeed not only possesses larger surface area per bone volume, but also is better vascularized than the cortical bone and shows a higher number of active osteoclasts [23]. Furthermore, on the nanoscopic scale, we believe that it can be resorbed faster than the cortical bone, due to its smaller and less organized mineral particles. Taken together our findings from different

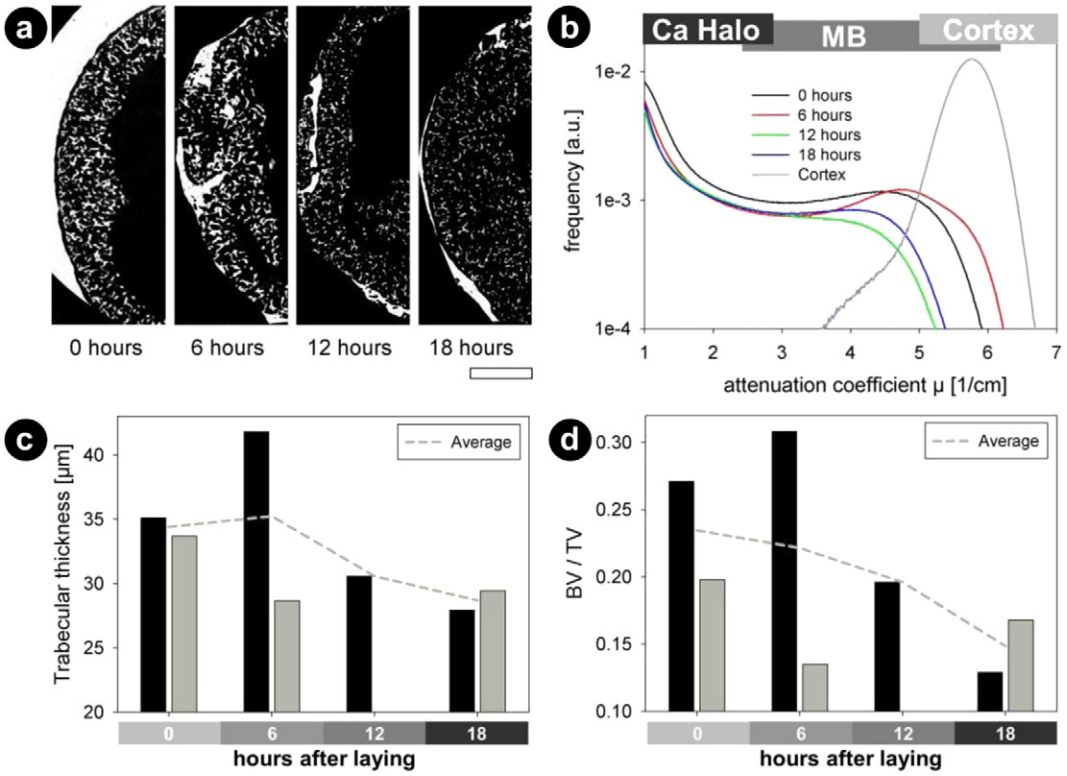

Fig. 4. Quantitative computer tomography of medullary bone at different time points of the oviposition cycle. (a) Representative images showing medullary bone structures at different time points with relatively thick and dense medullary bone trabeculae during the early stages (0, 6 h) as compared to later stages (12, 18 h). Thick, bright structures are parts of the cortical bone. (b) Distribution of the measured attenuation coefficient of medullary bone material at different time points (1 representative animal each) during the oviposition cycle. The attenuation coefficient correlates with the mineral content of bone structures. During all time points, high amounts of low mineralized tissue are present which represents freshly deposited bone material and calcium in the marrow space between trabeculae (calcium halo) and thus indicates high bone turnover rates. The mineral content of medullary bone is relatively high during oviposition (0 h) with a further increase of mineral content up to 6 h after oviposition. During the later stages (12, 18 h) degree of mineralization of medullary bone structures is strongly decreased. The grey curve denotes the cortex as a reference measure, showing higher mineral content. (c) Analysis of the average trabecular thickness at different time points for two animals per time point (except for 12 h). At later time points, trabeculae appear to be thinner. (d) Analysis of medullary bone volume fraction (BV/TV) ratio at different time points for two animals per time point (except for 12 h). At later time points, BV/TV appears to decrease. Scale bar is 1 mm.

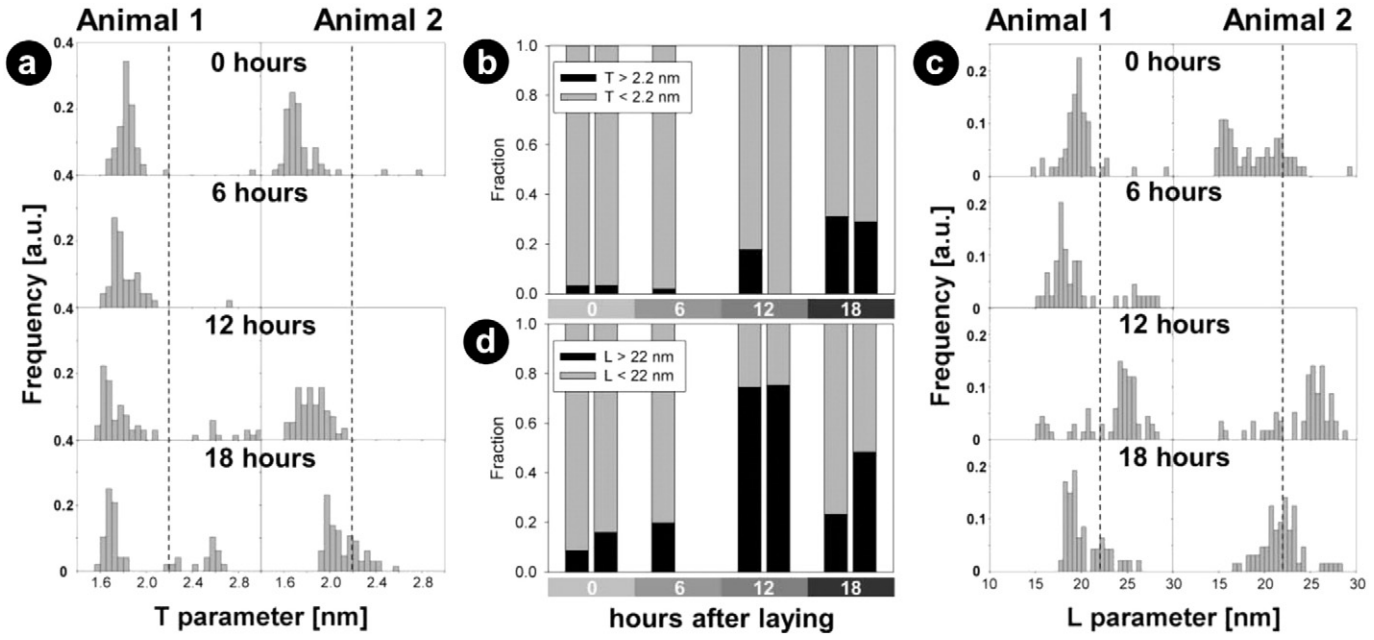

Fig. 5. (a) Alteration of medullary bone mineral particle thickness parameter (T) and (c) mineral particle length parameter (L) during the oviposition cycle measured in two different animals per time point (except 6 h). Histograms show the relative frequency of individual T and L parameters. Histograms are grouped into two fractions of thick versus thin and short versus long mineral particles with a threshold of 2.2 nm for the particle thickness and 22 nm for the particle length. The relative change of the two fractions is shown in (b) for the T parameter and in (d) for the L parameter. Low alteration in the T parameter with highest fraction of thick mineral in the late period, 18 h after laying. Alteration in the L parameter is strongly pronounced with a highest fraction of long mineral particles in the period around 12 h after laying.

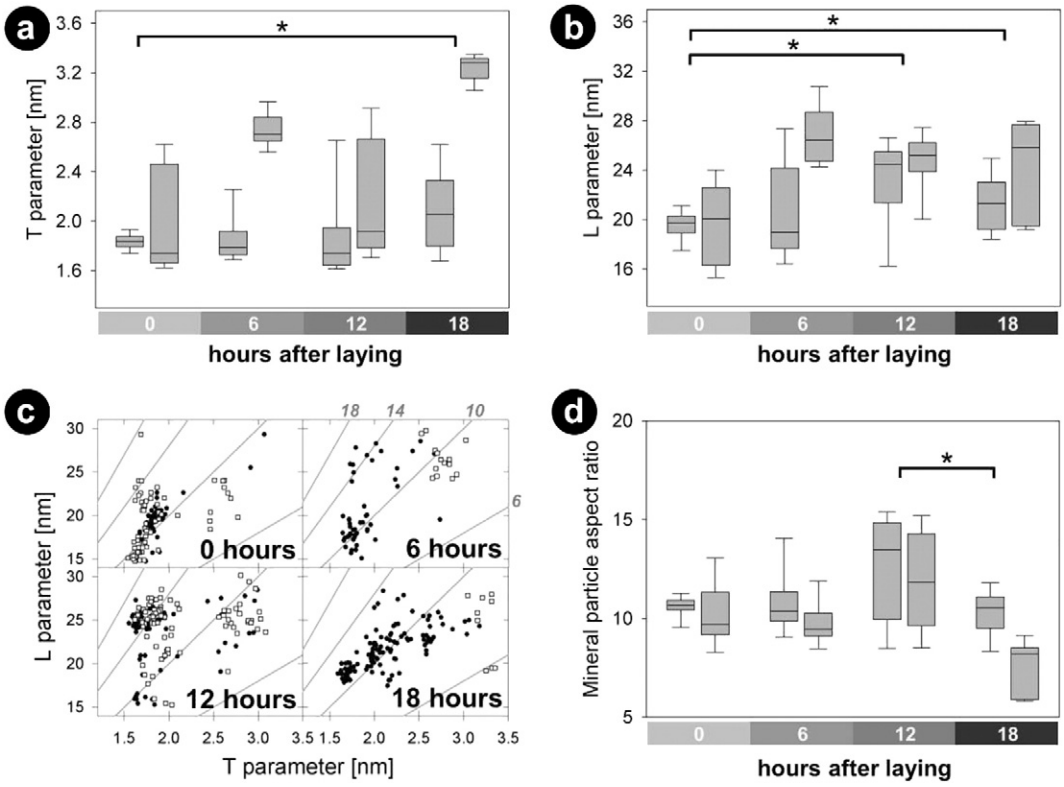

Fig. 6. Alteration of the mineral particle thickness, length and mineral particle aspect ratio during the oviposition cycle for n = 2 per time point. (a) Mineral particle thickness parameter showing no obvious trend and (b) mineral particle length parameter. Interestingly, animals with large T parameter also show large L parameter. To find an intrinsic normalization of the L to the T parameter (c) L is plotted vs. the T parameter for different time points. Black points and white squares depict animal 1 and animal 2, respectively. Lines are a guide to the eye depicting different L/T ratios (of 6, 10, 14 and 18) describing the mineral particle aspect ratio. A strong alteration of the mineral particle length over time with highest L values in the period around 12 h after oviposition is observed. (d) Plot of the average mineral particle aspect ratio at different time points of the oviposition cycle for each animal. Aspect ratio is highest in the period around 12 h after oviposition. * denotes a statistically significant difference of $P < 0.05$.

length scales, we have shown that microscopic and nanoscopic medullary bone mineral attributes significantly differ from chicken cortical bone. Due to its unique architecture, medullary bone facilitates a fast-responding system for calcium storage, mobilization and transportation and thus serves the metabolic calcium demands during the oviposition cycle. Due to its extremely efficient calcium metabolism, this system is the ideal candidate to study the complex interplay between bone cells and bone material and to better understand mechanisms involved during the formation and resorption of the bone.

Acknowledgments

We thank J. Mahamid, Y. Asscher, S. Weiner and L. Addadi from the Weizmann Institute of Science, Israel for the experimental support and fruitful discussions and A. Shipov, J. Milgram from the Hebrew University of Jerusalem, Israel for the support in sample collection. We are grateful to P. Kollmannsberger and R. Weinkamer for the valuable scientific discussions. We also thank E. Di Cola and M. Burghammer from the ESRF, France, C. Li and S. Siegel from the Max Planck Institute of Colloids and Interfaces, Germany and H. Riesemeier from the Federal Institute for Materials Research and Testing (BAM), Germany for their beamline support. We acknowledge having been granted beamtimes at the ESRF, France and at BAMline and the μSpot beamline at BESSY, HZB, Berlin. MK is funded by Bundesministerium für Bildung und Forschung (BMBF, grant-number: 01 EC 1006C, project 9133) and by the Minerva Foundation. PZ is grateful for funding by SPP 1420 of the DFG.

Appendix A. Supplementary data

Supplementary data to this article can be found online at http://dx.doi.org/10.1016/j.bone.2014.08.019.

References

[1] Currey JD. Bones: structure and mechanics. Oxford, UK: Princton University Press; 2002.
[2] Ruffoni D, Fratzl P, Roschger P, Klaushofer K, Weinkamer R. The bone mineralization density distribution as a fingerprint of the mineralization process. Bone 2007;40(5):1308–19.
[3] Roschger P, Paschalis E, Fratzl P, Klaushofer K. Bone mineralization density distribution in health and disease. Bone 2008;42(3):456–66.
[4] Mahamid J, Aichmayer B, Shimoni E, Ziblat R, Li CH, Siegel S, et al. Mapping amorphous calcium phosphate transformation into crystalline mineral from the cell to the bone in zebrafish fin rays. Proc Natl Acad Sci U S A 2010;107(14):6316–21.
[5] Mahamid J, Sharir A, Gur D, Zelzer E, Addadi L, Weiner S, et al. Bone mineralization proceeds through intracellular calcium phosphate loaded vesicles: a Cryo-electron Microscopy Study. J Struct Biol 2011;174(3):527–35.
[6] Fratzl P, Schreiber S, Klaushofer K. Bone mineralization as studied by small-angle X-ray scattering. Connect Tissue Res 1996;34(4):247–54.
[7] Boonrungsiman S, Gentleman E, Carzaniga R, Evans ND, McComb DW, Porter AE, et al. The role of intracellular calcium phosphate in osteoblast-mediated bone apatite formation. Proc Natl Acad Sci 2012;109(35):14170–5.
[8] Robinson RA. An electron-microscopic study of the crystalline inorganic component of bone and its relationship to the organic matrix. J Bone Joint Surg 1952;34(2):389–476.
[9] Weiner S, Price PA. Disaggregation of bone into crystals. Calcif Tissue Int 1986;39(6):365–75.
[10] Fratzl P, Groschner M, Vogl G, Plenk H, Eschberger J, Fratzl-Zelman N, et al. Mineral crystals in calcified tissues: a comparative study by Saxs. J Bone Miner Res 1992;7(3):329–34.

[11] Nesbitt SA, Horton MA. Trafficking of matrix collagens through bone-resorbing osteoclasts. Science 1997;276(5310):266–9.
[12] Salo J, Lehenkari P, Mulari M, Metsikko K, Vaananen HK. Removal of osteoclast bone resorption products by transcytosis. Science 1997;276(5310):270–3.
[13] Kawahara I, Koide M, Tadokoro O, Udagawa N, Nakamura H, Takahashi N, et al. The relationship between calcium accumulation in osteoclast mitochondrial granules and bone resorption. Bone 2009;45(5):980–6.
[14] Bar A. Calcium transport in strongly calcifying laying birds: mechanisms and regulation. Comp Biochem Physiol A Mol Integr Physiol 2009;152(4):447–69.
[15] Edelstein S, Harell A, Bar A, Hurwitz S. Functional metabolism of vitamin-D in chicks fed low-calcium and low-phosphorus diets. Biochim Biophys Acta 1975;385(2):438–42.
[16] Fratzl P, Gupta HS, Paris O, Valenta A, Roschger P, Klaushofer K. Diffracting "Stacks of Cards"—some thoughts about small-angle scattering from bone. Scattering methods and the properties of polymer materials. Springer; 2005 33–9.
[17] Fratzl P, Gupta H, Paschalis E, Roschger P. Structure and mechanical quality of the collagen—mineral nano-composite in bone. J Mater Chem 2004;14(14):2115–23.
[18] Schweitzer MH, Elsey RM, Dacke CG, Horner JR, Lamm ET. Do egg-laying crocodilian (Alligator Mississippiensis) archosaurs form medullary bone? Bone 2007;40(4):1152–8.
[19] Shipov A, Sharir A, Zelzer E, Milgram J, Monsonego-Ornan E, Shahar R. The influence of severe prolonged exercise restriction on the mechanical and structural properties of bone in an Avian Model. Vet J 2010;183(2):153–60.
[20] Fratzl P, Weinkamer R. Nature's hierarchical materials. Prog Mater Sci 2007;52(8):1263–334.
[21] Barak MM, Weiner S, Shahar R. The contribution of trabecular bone to the stiffness and strength of rat lumbar vertebrae. Spine 2010;35(22):E1153–9.
[22] Dacke CG, Arkle S, Cook DJ, Wormstone IM, Jones S, Zaidi M, et al. Medullary bone and avian calcium regulation. J Exp Biol 1993;184:63–88.
[23] Van de Velde J, Vermeiden J, Touw J, Veldhuijzen J, et al. Changes in activity of chicken medullary bone cell populations in relation to the egg-laying cycle. Metab Bone Dis Relat Res 1984;5(4):191–3.
[24] Weiner S, Bar-Yosef O. States of preservation of bones from prehistoric sites in the near-east—a survey. J Archaeol Sci 1990;17(2):187–96.
[25] Paris O, Li CH, Siegel S, Weseloh G, Emmerling F, Riesemeier H, et al. A new experimental station for simultaneous X-ray microbeam scanning for small- and wide-angle scattering and fluorescence at Bessy Ii. J Appl Crystallogr 2007;40:S466–70.
[26] Rinnerthaler S, Roschger P, Jakob H, Nader A, Klaushofer K, Fratzl P. Scanning small angle x-ray scattering analysis of human bone sections. Calcif Tissue Int 1999;64(5):422–9.
[27] Lange C, Li C, Manjubala I, Wagermaier W, Kuhnisch J, Kolanczyk M, et al. Fetal and postnatal mouse bone tissue contains more calcium than is present in hydroxyapatite. J Struct Biol 2011;176(2):159–67.
[28] Rack A, Zabler S, Mueller BR, Riesemeier H, Weldemann G, Lange A, et al. High resolution synchrotron-based radiography and tomography using hard X-rays at the Bamline (Bessy Ii). Nucl Inst Methods Phys Res A 2008;586(2):327–44.
[29] Mirone A, Wilcke R, Hammersley A, Ferrero C. High speed tomographic reconstruction. from http://www.esrf.eu/UsersAndScience/Experiments/TBS/SciSoft/; 2009.
[30] Doube M, Klosowski MM, Arganda-Carreras I, Cordelieres FP, Dougherty RP, Jackson JS, et al. BoneJ free and extensible bone image analysis in ImageJ. Bone 2010;47(6):1076–9.
[31] Yair R, Uni Z. Content and uptake of minerals in the yolk of broiler embryos during incubation and effect of nutrient enrichment. Poult Sci 2011;90(7):1523–31.
[32] Luck M, Scanes C. Plasma levels of ionized calcium in the laying hen (*Gallus Domesticus*. Comp Biochem Physiol A Physiol 1979;63(1):177–81.
[33] Miller SC. Rapid activation of the medullary bone osteoclast cell surface by parathyroid hormone. J Cell Biol 1978;76(3):615–8.
[34] King GJ, Holtrop ME, Raisz LG. The relation of ultrastructural changes in osteoclasts to resorption in bone cultures stimulated with parathyroid hormone. Metab Bone Dis Relat Res 1978;1(1):67–74.
[35] Omelon S, Georgiou J, Henneman ZJ, Wise LM, Sukhu B, Hunt T, et al. Control of vertebrate skeletal mineralization by polyphosphates. Plos One 2009;4(5):16.
[36] Singh R, Joyner CJ, Peddie MJ, Taylor TG. Changes in the concentrations of parathyroid hormone and ionic calcium in the plasma of laying hens during the egg cycle in relation to dietary deficiencies of calcium and vitamin D. Gen Comp Endocrinol 1986;61(1):20–8.
[37] Taylor TG, Belanger L. The mechanism of bone resorption in laying hens. Calcif Tissue Res 1969;4(1):162–73.
[38] Dacke CG, Furr B, Boelkins JN, Kenny AD. Sexually related changes in plasma calcitonin levels in Japanese quail. Comp Biochem Physiol A Physiol 1976;55(4):341–4.
[39] Teitelbaum SL. Bone resorption by osteoclasts. Science 2000;289(5484):1504–8.
[40] Mahamid J, Addadi L, Weiner S. Crystallization pathways in bone. Cells tissues organs 2011;194(2–4):92–7.
[41] Weiner S, Addadi L. Crystallization pathways in biomineralization. Annu Rev Mater Res 2011;41:21–40.
[42] Hurwitz S. Calcium turnover in different bone segments of laying fowl. Am J Physiol Leg Content 1965;208(1):203–7.
[43] Simkiss K. Calcium in reproductive physiology. Chapman and Hall/Reinhold; 1967.